Wasige, E., Alharbi, K. H., Al-Khalidi, A., Wang, J., and Khalid, A. (2017) Resonant Tunnelling Diode Terahertz Sources for Broadband Wireless Communications. In: Terahertz, RF, Millimeter, and Submillimeter-Wave Technology and Applications X, San Francisco, CA, USA, 28 Jan - 2 Feb 2017, (doi:10.1117/12.2256357)
This is the author's final accepted version.

There may be differences between this version and the published version. You are advised to consult the publisher's version if you wish to cite from it.

http://eprints.gla.ac.uk/135942/

Deposited on: 31 January 2017

Enlighten – Research publications by members of the University of Glasgow
http://eprints.gla.ac.uk33640

Resonant Tunnelling Diode Terahertz Sources for Broadband Wireless Communications

Edward Wasige*[a], Khalid H. Alharbi[a], Abdullah Al-Khalidi[a], Jue Wang[a], Ata Khalid[a], Gil C. Rodrigues[b], and José Figueiredo[b]
[a]High Frequency Electronics Group, School of Engineering, University of Glasgow, UK.
[b]Departamento de Física, Universidade do Algarve, Campus de Gambelas, 8005-139 Faro, Portugal.

*edward.wasige@glasgow.ac.uk; phone +44 141 330 8662; fax +44 141 330 4907; www.gla.ac.uk

ABSTRACT

This paper will discuss resonant tunnelling diode (RTD) sources being developed on a European project iBROW (ibrow.project.eu) to enable short-range multi-gigabit wireless links and microwave-photonic interfaces for seamless links to the optical fibre backbone network. The practically relevant output powers are at least 10 mW at 90 GHz, 5 mW at 160 GHz and 1 mW at 300 GHz and simulation and some experimental results show that these are feasible in RTD technology. To date, 75 - 315 GHz indium phosphide (InP) based RTD oscillators with relatively high output powers in the 0.5 – 1.1 mW range have been demonstrated on the project. They are realised in various circuit topologies including those that use a single RTD device, 2 RTD devices and up to 4 RTD devices for increasingly higher output power. The oscillators are realised using only photolithography by taking advantage of the large micron-sized but broadband RTD devices. The paper will also describe properties of RTD devices as photo-detectors which makes this a unified technology that can be integrated into both ends of a wireless link, namely consumer portable devices and fibre-optic supported base-stations (since integration with laser diodes is also possible).

Keywords: Terahertz sources, resonant tunneling diodes, wireless/photonic interfaces

1. INTRODUCTION

Terahertz (THz) radiation, whose frequency range lies between millimetre-waves and infrared light in the electromagnetic spectrum, has many potential applications in different scientific fields such as medical diagnostics, security imaging, and wireless communication[1,2]. However, because of the lack of efficient and practical THz radiation sources this part of the electromagnetic spectrum has been known as the THz gap. Most of the current THz electronic sources used today are based on low frequency sources with multiplier chains[3,4]. The efficiency of these architectures is low and the sources are not compact. There are also photonics-based THz sources: quantum cascade lasers (QCLs) and far infrared (FIR) gas lasers can operate in the THz gap[5-7] producing tens of milliwatt power, but they are bulky with QCLs requiring cryogenic cooling. Recently, QCL sources operating at room temperature and limited to frequencies above 1 THz have been demonstrated[7], but require high power to operate.

To realise compact and efficient THz sources, especially in the 0.1 - 3 THz range, a number of electronic devices including Gunn diodes, resonant tunneling diodes (RTDs) etc. have been considered. Of these, the InP-based resonant tunnelling diode (RTD) is the fastest electronic device and has the potential to construct compact oscillators that can operate up to 2.5 THz and at room temperature[8]. A number of demonstrations of the large RTD bandwidth have been reported recently[9-14]. Demonstrations of wireless transmission using RTD oscillators at 300 GHz[15], 500 GHz[16], and 350 GHz with intensity modulation up to 30 GHz bandwidth[17] have also been reported. These individual RTD oscillators, however, exhibit low output power in the microwatt range, partly due to using sub-micron RTD device sizes chosen to reduce the RTD self-capacitance[18]. For example, 150 µW output power was reported at 271 GHz[19], 0.4 µW was reported at 1.92 THz[9], and 1.9 µW was reported at 1.52 THz[12]. Also, higher powers ~400 µW at 530 – 590 GHz from a single oscillator and combined output powers of 610, 270, and 180 µW at 620, 770, and 810 GHz in a two-element array have been reported[20]. However, all prior work on THz RTD sources use integrated antennas and so the power measurements have to account for free space loss. As the antenna patterns are not well known with respect to measurement locations, the errors in reported output powers are difficult to quantify. For arrays of these free running

oscillators[20], the power may add up or subtract in free space and so the measurements can be very inaccurate. Nevertheless, high power levels in the milliwatt range are desirable. To provide a perspective for this, practically relevant output powers of at least 10 mW at 90 GHz, 5 mW at 160 GHz and 1 mW at 300 GHz are required[21], for example, for the future wireless indoor communications in femtocell scenarios[22], and these are yet to be demonstrated as single compact electronic sources in integrated circuit form.

To increase the output power of RTD oscillators, we have developed designs that employ the largest possible sized devices and also developed oscillator circuit topologies that employ two RTD devices. Using this approach, 28 GHz and 76 GHz InP-based RTD oscillators with around 1 mW were realized[23,24]. Thereafter, D-band oscillators operating at 125 GHz, 156 GHz and 166 GHz, with output power of 0.34 mW, 0.24 mW, 0.17 mW, respectively, were also demonstrated[25]. These oscillators used shorted coplanar waveguide (CPW) lines of characteristic impedance (Z_0) 50 Ω to realise the inductances required to resonate with the device self-capacitance for a given target oscillation frequency. However, for very high frequencies from the J-band, the length of the 50 Ω CPW line (shorted stub) becomes extremely small and so limits that maximum oscillation frequency. In this paper, we extend the previous work by investigating large RTD devices together with lower Z_0 CPW shorted stubs for oscillators with higher oscillation frequencies and higher power. Calculations show that using this approach the performance of RTD oscillators could be further improved and extended deeper into the THz regime.

The rest of the paper is organized as follows. In section 2, a discussion on RTD bandwidth, sizing and power considerations is presented first. Then a review of the conventional RTD device design for THz oscillators is provided and contrasted with the approach taken here. Details of the fabrication of RTD devices and their DC characteristics are also described. In section 3, the design and fabrication of RTD oscillators is described. The measurement setup for characterising the RTD oscillators is introduced in section 4, followed by discussion on the experimental results. Optoelectronic properties of RTDs are summarized in section 5, while conclusions with future work are given at the end of the paper in Section 6.

2. RTD DEVICE DESIGN, FABRICATION & CHARACTERISATION

2.1 Bandwidth, Device Sizing and Output Power Considerations

The device cut-off frequency (f_{max}) of an RTD can be estimated from (assuming $R_S << R_n$,)[26]:

$$f_{\max} \approx \frac{1}{2\pi C_n \sqrt{R_s R_n}} \tag{1}$$

where C_n is the self-capacitance of the device; R_n is absolute value of the (minimum) negative differential resistance of the device; and R_S accounts for the contact and access parasitic resistances. Note from (1) that f_{max} can be increased through contradictory requirements, either as is usually done by reducing C_n (through decreasing device size) or as proposed here by lowering R_n and R_s (through increasing device size).

The resistance R_n can be estimated from $R_n = \frac{2\Delta V}{3\Delta I}$ where $R_n = 1/G_n$ is the negative differential conductance (NDC), ΔI and ΔV are the peak-to-valley current and voltage differences, respectively. A figure-of-merit for RTDs is the peak current density (J_P), the (maximum) current at which the device starts to exhibit NDC. Since ΔV is usually fixed by the epitaxial layer structure, to realise a device of a given NDC (which can be defined by G_n), the device has to be sized accordingly. G_n is usually chosen under 50 mS. Beyond about 100 mS, the NDC impedance level drops to a few Ohms (< -10 Ω) and this region is difficult/impossible to discern or measure. As such high J_P structures necessarily require small RTD devices sizes. Further, to avoid oscillations of the bias circuit/lines when the device is biased in the NDC region, a shunt resiatnce R_e (with $R_n > 1/G_n$) can be connected across the device, which for a given R_e establishes the maximum device size[23], A_{max}, as

$$A_{\max} R_e < \frac{2\Delta V}{3\Delta J} \tag{2}$$

where ΔJ is the peak-to-valley current density difference. R_e usually chosen to be in the 10-20 Ω range[27].

The RTD model, and in particular the device capacitance C_n, is extracted from DC and S-parameter measurements[28,29],

while the theoretical maximum generated power (P_{max}) of a single RTD device oscillator oscillating at frequency f_{osc} can be estimated from the device's I-V characteristics and f_{max} using the formula[26]:

$$P_{\max}\left(f_{osc}\right) \approx \frac{3}{16}\Delta V \Delta I\left(1-\frac{f_{osc}^{2}}{f_{\max}^{2}}\right) \tag{3}$$

RTDs for use in high power oscillators should therefore be designed to maximize both ΔV and ΔI, with the epitaxial layer structure designed to maximize ΔV while the use of larger area (with low C_n) devices adopted to maximise ΔI.

2.2 Device design considerations

The RTD device consists of a narrow bandgap material (4.5 - 6 nm thick $In_{0.53}Ga_{0.47}As$ quantum well) sandwiched between two thin wide bandgap materials (1 - 3 nm AlAs barriers), making up the double barrier quantum well (DBQW) structure. The structure is completed by un-doped or lightly doped $In_{0.53}Ga_{0.47}As$ spacer layers, n-type emitter/collector layers and highly doped $In_{0.53}Ga_{0.47}As$ contact layers on either side of the DBQW.

High peak current density (J_P) (> 6 mA/µm^2) device designs have conventionally been used for THz RTDs since they require the use of submicron device sizes with correspondingly small device self-capacitances [12-14, 18], but they are actually best suited for switching applications[30]. They typically employ ~1 nm AlAs barriers. However, such thin barrier thicknesses reduce the peak-to-valley current ratio (PVCR) to less than two (2) through the increased electron transmission probability through the DBQW. Therefore, the peak-to-valley current difference reduces and so does the potential output power of an oscillator using such a device. Besides, the accurate growth of such ultra-thin AlAs barriers is difficult/challenging leading to potential non-uniformity of the epi-layer structure and so limiting the repeatability, reproducibility, and manufacturability of the devices[31,32]. Other issues that may be attributed to high J_P RTDs include reduced thermal stability[18,30] and the need for ultra-low Ohmic specific contact resistances for the small-sized devices to keep the device contact resistance low[33], since high resistance limits the oscillator output power significantly[26,27]. Last but not least, small devices in the sub-micrometer range require electron-beam lithography, which is more costly compared to fabrication of larger devices with photolithography.

Lower J_P designs as those used in mm-wave oscillators[23-25], on the other hand, employ large micro-sized RTD devices and so can provide high RF power in oscillator circuits due to the increased ΔI, do not suffer thermal stability issues and can be fabricated with photolithography. Such devices employ thicker barrier layers (>1.4 nm). The epitaxial growth requirements are therefore less demanding and more accurate benefiting a more reproducible technology. PVCR is also higher (>3), and since for a given specific contact resistance, the larger size RTD devices exhibit low Ohmic contact resistance, these factors benefit higher output power in oscillator circuits[26]. Crucially, though, is that both the lower J_P, e.g. Ref. [23]-[25], and higher J_P , e.g. Ref. [14], [18], have low and comparable device self-capacitances in the 2-4 fF/µm^2 range so lower J_P structures can also enable the realisation of THz oscillators.

2.3 Device fabrication and characterisation

The epi-layer structure of the RTD wafer that was used in the oscillators reported here was grown by molecular beam epitaxy (MBE) by IQE Ltd on a semi-insulating InP substrate. It employs a 4.5 nm $In_{0.53}Ga_{0.47}As$ quantum well, 1.4 nm AlAs barriers and 25 nm spacers. This DBQW design offers current density J_P of ~3 mA/µm^2 but large PVCR (>3.5). The collector and emitter layers are made of highly doped $In_{0.53}Ga_{0.47}As$ material (3×10^{19} cm^{-3}) doped with Si. The RTD devices were fabricated using optical lithography techniques. Two RTD with two different mesa sizes, 4 µm × 4 µm and 3 µm × 3 µm chosen according to (2), were fabricated. Chemical wet etching (H_3PO_4:H_2O_2:H_2O = 1:1:38) was used to define the RTD mesa. This recipe has an etching rate of around 100 nm/min. Polyimide PI-2545 was used for device passivation. The epitaxial structure has an estimated capacitance per unit area of 3.56 fF/µm^2. Therefore, the self-capacitances for 3 µm × 3 µm and 4 µm × 4 µm were 32 fF and 57 fF, respectively, and are low enough to allow the realization of mm-wave/THz oscillators. The measured specific contact resistance ρ was 52 Ω-µm^2 giving f_{max} of 340 GHz and 390 GHz for the 3 µm × 3 µm and the 4 µm × 4 µm devices, respectively.

3. OSCILLATORS DESIGN AND FABRICATION

As already noted, for each RTD device, there is a limitation on the maximum mesa size (A_{max}) for which bias oscillations can be eliminated with a shunt resistor, R_e. The used oscillator topology in this work employs two individually biased and stabilised RTD devices and a single RF load as shown in Fig. 1(a). The circuit potentially provides double the RF output power of a single RTD device oscillator using an identical RTD device. Each RTD device is also connected to a bypass capacitor C_e which is placed to short-circuit the RF signal to ground and avoid dissipating the RF power over R_e. This capacitor also provides a short-circuit termination for a CPW transmission line used to realise inductance L which is designed to resonate with the RTD self-capacitance C_n to obtain the desired frequency. A shorted transmission line acts as an inductance when its electrical length is less than 90º and the natural/lowest oscillation frequency of the circuit is such that this is always the case. The resistance R_L represents the load, 50 Ω in our case, which is introduced by the spectrum analyser or power meter during measurement. Capacitors (DC-block) are introduced in the circuit to prevent any DC from reaching the spectrum analyzer during on-wafer measurements. The inductor L_b denotes the bias cable inductance.

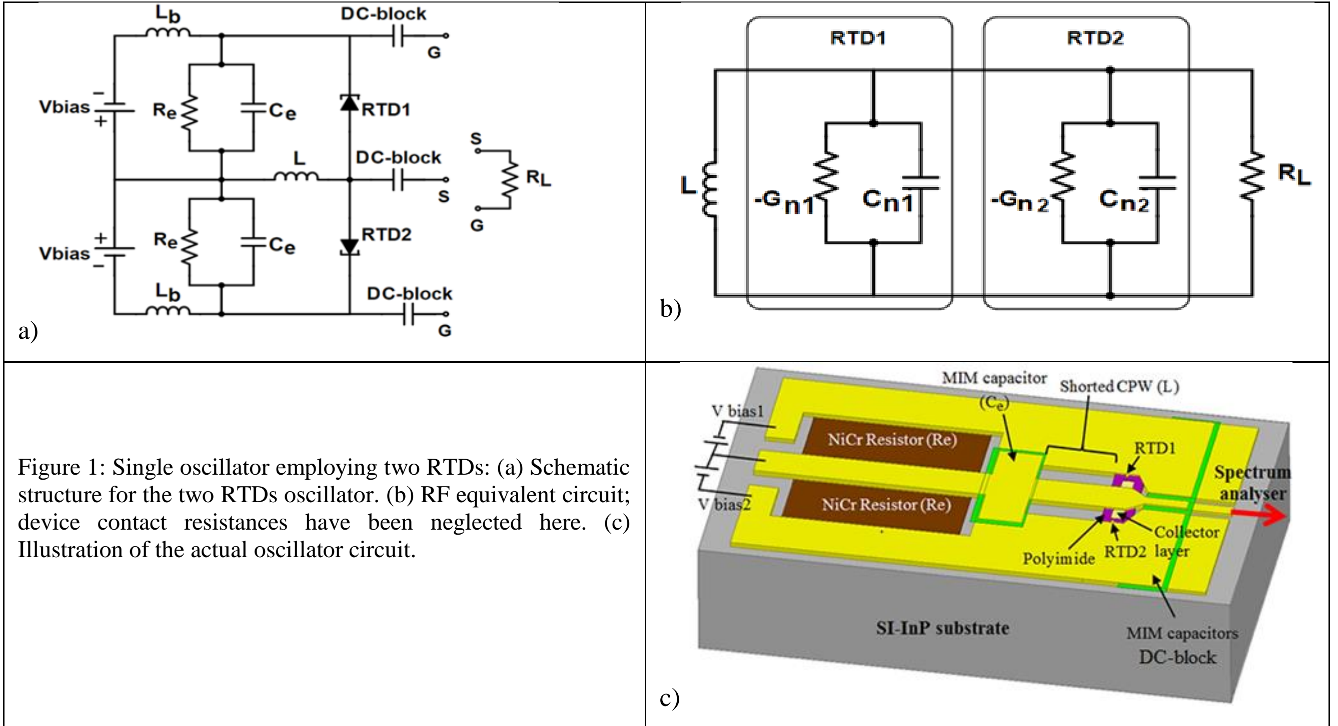

Figure 1: Single oscillator employing two RTDs: (a) Schematic structure for the two RTDs oscillator. (b) RF equivalent circuit; device contact resistances have been neglected here. (c) Illustration of the actual oscillator circuit.

The RF equivalent circuit of the two RTD oscillator is shown Fig. 1b where each RTD is modeled by its lumped small signal equivalent circuit comprising the negative differential conductance ($-G_{n1}$ and $-G_{n2}$) in parallel with the self-capacitance (C_{n1} and C_{n2}) of each device. The device contact resistance is neglected in this description for simplicity. The oscillation frequency for this parallel resonant circuit is given by $f_{osc} = \dfrac{1}{2\pi\sqrt{(c_{n1}+C_{n2})L}}$.

As the 9 or 16 μm^2 RTDs are the smallest components in the oscillator circuits, photolithography is used to define all features during circuit fabrication. The layout was designed by L-Edit software. The stabilizing resistor R_e was realised from a 33 nm thin film NiCr (60:40) which has a sheet resistance of 50 Ω/square. The designed resistor value was 22 Ω, realised with dimensions of 300 µm × 130 µm and the measured value from process control structures (PCM) was within ±10%. Metal-insulator-metal (MIM) capacitors were designed and fabricated to realise C_e and the DC-blocks in the circuits. The dielectric layer used was Si_3N_4 with 75 nm thickness, which corresponds to 0.8 fF/µm^2. It was deposited using inductively coupled plasma (ICP) chemical vapor deposition (CVD). The designed value of C_e was 10 pF realised

with MIM size of 210 µm × 60 µm) and that of DC-Block capacitor was 800 fF realised with MIM size of 20 µm × 80 µm. Measurements of PCM structures confirmed that the realised structures had expected values[34]. The inductance L was realised by appropriate lengths of CPW transmission lines with Z_0 of 25 Ω, 32 Ω, or 50 Ω shorted by the bypass capacitor C_e. For the 25 Ω, 32 Ω, and 50 Ω CPW lines, the signal lines widths are 126 µm, 110 µm, and 60 µm and the gap distances between the signal lines to the ground planes are 7 µm, 15 µm, and 40 µm, respectively. Modelling of the passive parts, such as the resonating inductance and MIM capacitors, was done through both High Frequency Structural Simulator (HFSS) and validation of the models dove via S-parameter measurements[34]. An illustration of the two RTD device oscillator is shown in Fig. 1c.

4. OSCILLATOR MEASUREMENT

4.1 Measurement Setups

The fabricated oscillators were measured on-wafer by using Keysight E4448A spectrum analyzer, with biasing provided through a ground-signal-ground (GSG) Cascade probe. The schematic diagram of the measurement setup is shown in Fig. 2(a). It consists of a J-band (220 – 325 GHz) 50 µm pitch GSG probe, a J-band harmonic mixer (Farran Technology WHM-03) to mix down the signal. A diplexer is used to separate the local oscillator (LO) and intermediate frequencies (IF). With the built-in signal identification function of the spectrum analyzer, the oscillation frequency was accurately identified. The mixer loss is specified by the manufacturer to be approximately 50 dB for the J-band. As calibration of this is however non-trivial (reference sources at the desired frequencies are not easily available), we considered the mixer to be non-calibrated, and so the actual output power was measured by a calibrated power meter (Erikson PM4). Since the input of power sensor head is WR-10 (W-band) waveguide, a WR-3 to WR-10 tapered waveguide was used as shown in Fig. 2b, and therefore losses due to the probe (3 dB) and waveguide (0.5 dB) were taken into account. Fig. 2c shows one of the fabricated oscillators during on-wafer characterisation.

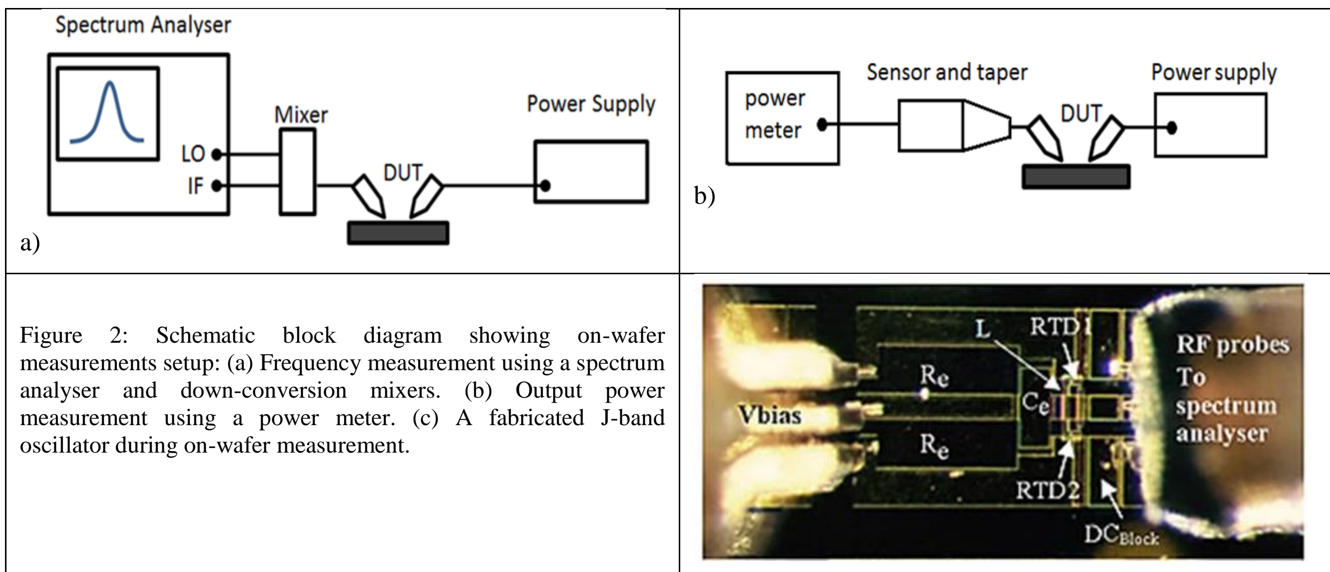

Figure 2: Schematic block diagram showing on-wafer measurements setup: (a) Frequency measurement using a spectrum analyser and down-conversion mixers. (b) Output power measurement using a power meter. (c) A fabricated J-band oscillator during on-wafer measurement.

As the characterization of THz oscillators using a 50 GHz spectrum analyser with down conversion mixers is time consuming and non-trivial, a recently developed quicker technique which uses a vector network analyser (VNA) was used to identify the oscillation frequencies of the circuits[35]. These were therefore known prior to using the spectrum analyser for detailed characterization. Nonetheless, it is useful to point out that as part of the standard characterization methodology for the oscillators, initially the output is connected directly to a 50 GHz spectrum analyser to ascertain if any oscillations up to this frequency are being generated; and then with appropriate down conversion mixers, the higher bands (V-, W- and G-bands) are also checked and so the observed frequencies are deemed to be the true fundamental oscillation frequencies.

4.2 Oscillation Frequency Results

Different oscillators, each employing either two 4 µm × 4 µm or 3 µm × 3 µm RTD devices, with different Z_0 CPW shorted stubs were fabricated and characterised. Two different samples from two different runs labelled sample-1 and sample-2 were fabricated to investigate the repeatability and reproducibility of the process by monitoring the oscillators' performance. Example/typical frequency measurements from sample1 are summarized here. Figure 3a shows the detected signal for a 308 GHz oscillator using the VNA[35] and spectrum analyser techniques when V_{bias} = 1.42 V and I_{bias} = 176 mA. It employs two 4 µm ×4 µm RTDs and a 10 µm long 25 Ω CPW shorted stub. The sharp reversal in the return loss in Fig. 3a, from under -10 dB to about 8 dB in this case, is known to indicate the existence of an external oscillation frequency being sensed by the VNA. Figure 3b shows the spectrum of the same oscillator measured using the spectrum analyser.

A variety of oscillation frequencies were observed for different CPW lengths and impedances. For other oscillator employing two 4 µm ×4 µm RTDs, a 3 µm long 50 Ω CPW shorted stub circuits showed an oscillation frequency of 304 GHz, while for an oscillator with 7 µm long 50 Ω CPW shorted stub, the oscillation frequency was 245 GHz. A higher oscillation frequency of 309 GHz was observed from oscillator with same (7 µm) CPW length but with Z_0 = 25 Ω, as expected. And, an oscillation frequency of 254 GHz was measured for 8 µm long 32 Ω CPW shorted stub. These results demonstrate that large RTD devices and longer lower Z_0 transmission lines can be employed and fabricated accurately using photolithography to realise THz RTD oscillators.

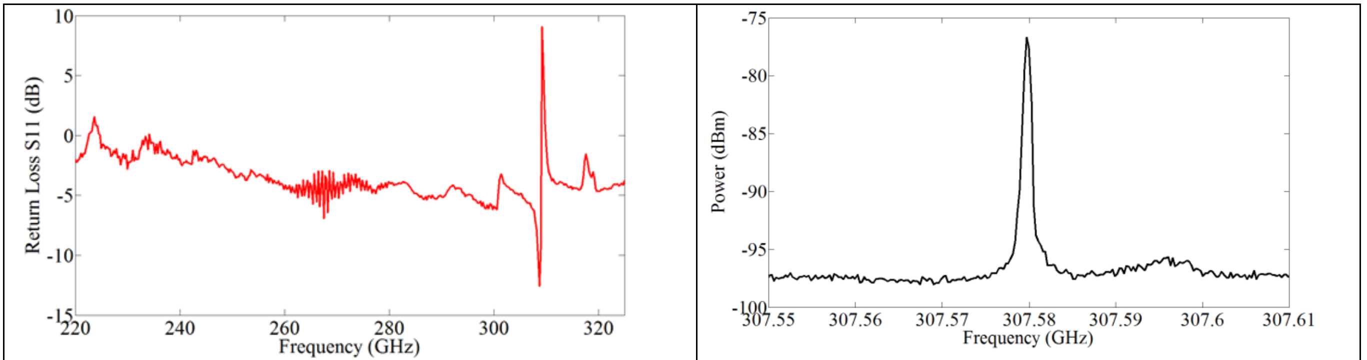

Figure 3: Measured spectrum of the 308 GHz oscillator. (a) Frequency detection technique using VNA showing gain at 308 GHz. (b) Measured spectrum using spectrum analyser.

4.3 Oscillators Output Power Results

The oscillator output power measurements were made using the setup in Figure 2(b), using the J-band (220 – 325 GHz) rectangular waveguide measurement system. Figure 4 shows the measured output power versus bias for the 308 GHz oscillator which employs two 4 µm × 4 µm RTDs. There is relatively little variation with bias for the oscillators on sample-2. Note that the output power data shown in Figure 4 has been compensated the probe and taper insertion losses which is 3.5 dB as per manufacturer specifications, while the spectrum shown in Fig. 3b is the actual measured trace. Using the power measured by the power meter, the losses of the frequency measurement setup which uses the spectrum analyser was estimated to be approximately 72 dB which accounts for the probe losses, mixer loss, waveguide losses and IF cabling losses. The DC to RF conversion efficiency for all oscillators was under 0.2%. Future work will consider advanced bias stabilisation criteria/circuit so as to avoid the large DC power dissipated in R_e [36]. Note also that the relatively high measured output powers indicate that the cut-off frequencies for the devices may be much higher than predicted by (1).

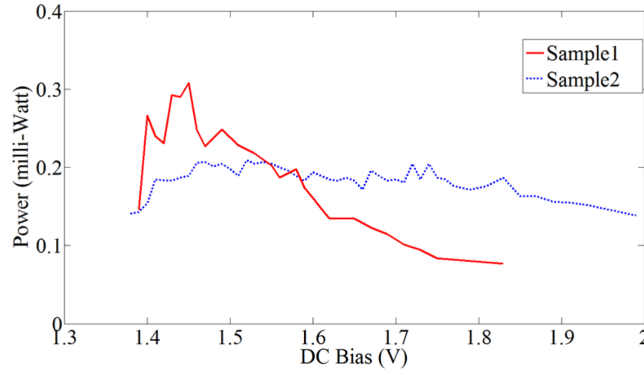

Figure 4: Measured output power of the 308 GHz oscillators versus bias voltage.

Table 1 compares the measured highest oscillator output power in this work with SiGe HBT, Gunn diode, InP DHBT and CMOS technologies for which on-wafer probing measurement setup was also used. The RTD oscillator compares well in terms of output power even though presently the DC power consumption is high. The key advantages for RTDs are the reduced lithography requirements and the simple circuitry for THz sources.

Table 1: Comparison of RTD oscillators with other on-wafer probed THz oscillators.

Frequency (GHz)	**Power (dBm)**	**DC Power (mW)**	**Technology**	**Ref.**
284	-3.4	250	3 μm × 3 μm RTD	This work
367	-8	64	130 nm SiGe	[37]
307	-15.5	196	$In_{0.53}Ga_{0.47}As$ planar Gunn diode	[38]
310	-6.2	76	256 nm InP DHBT	[39]
290	-1.2	325	65 LP bulk CMOS	[40]

Figure 5 shows the estimated oscillation frequency versus different Z_0 CPW shorted stubs and different RTD device sizes that could be considered for implementation in new oscillator circuits. They show that 10 μm 25 Ω CPW long lines can be used to realise oscillators up to about 600 GHz; and oscillators with extremely short 2 μm lines can reach up to 1.4 THz. To achieve these high frequencies, the device cut-off frequency needs to be extended and this can be achieved through lower resistance Ohmic contacts, for instance, by using a high indium content contact layer to realise very low specific contact resistance (ρ) as already demonstrated by others [41]. For example, 2.9 THz and 3.25 THz are estimated using equation (1) for the 3 μm × 3 μm and the 4 μm × 4 μm devices, respectively, if ρ = 0.73 Ω-μm^2 (reported in Ref. [42]) was successfully realised. As already noted, equation (1) shows that the cut-off frequency (f_{max}) can be increased by reducing R_s and R_n, both of which can be realised by using larger mesa area RTD devices. Careful epitaxial layer design may also help offset the increased device capacitance from the larger devices.

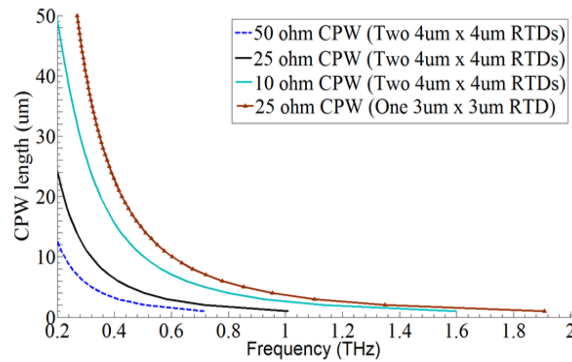

Figure 5: Calculated oscillation frequency versus CPW length.

5. RTD-BASED OPTOELECTRONIC CIRCUITS

The operation and functionality of a considerable number of new optoelectronic devices and circuits based on III-V semiconductor compound materials can benefit from the integration with DBQW-RTDs taking advantage of the negative differential conductance (NDC) produced by the DBQW structures. Such optoelectronic devices include laser diodes, semiconductor optical amplifiers, photo-detectors, and semiconductor electro-refraction and electro-absorption modulators. Particularly, the integration of DBQWs with unipolar photodetectors by embedding the DBQW within or close to the light sensitive region gives rise to a new device known from now as resonant tunneling diode photodetector (RTD-PD)[43-45].

RTD-PDs for operation at 1300 nm and 1550 nm were implemented with various optical windows sizes and shapes. The RTD-PD epi-layer was grown on SI-InP, comprising 1.7 nm AlAs barriers and 5.7 nm quantum well, two InGaAlAs light absorbing layers 500 nm thick each side of the DBQW, and two InAlAs light layers. Figure 6(a) illustrates the energy bands schematic diagram of an RTD-PD obtained by the integration of an InGaAs/AlAs DBQW with a unipolar InGaAlAs/InAlAs photoconductive structure lattice matched to InP. Figure 6(b) shows typical current-voltage characteristics under dark and illuminated conditions, where a global shift of the I-V to lower voltage induced by the light absorption is clearly visible. Figure 6(c) represents the responsivity of the devices as function of the applied voltage. An intensity modulated light can induced peak to valley switching giving rise to a current change equivalent to the peak-to-valley current difference which can lead to absolute responsivities of tens of A/W.

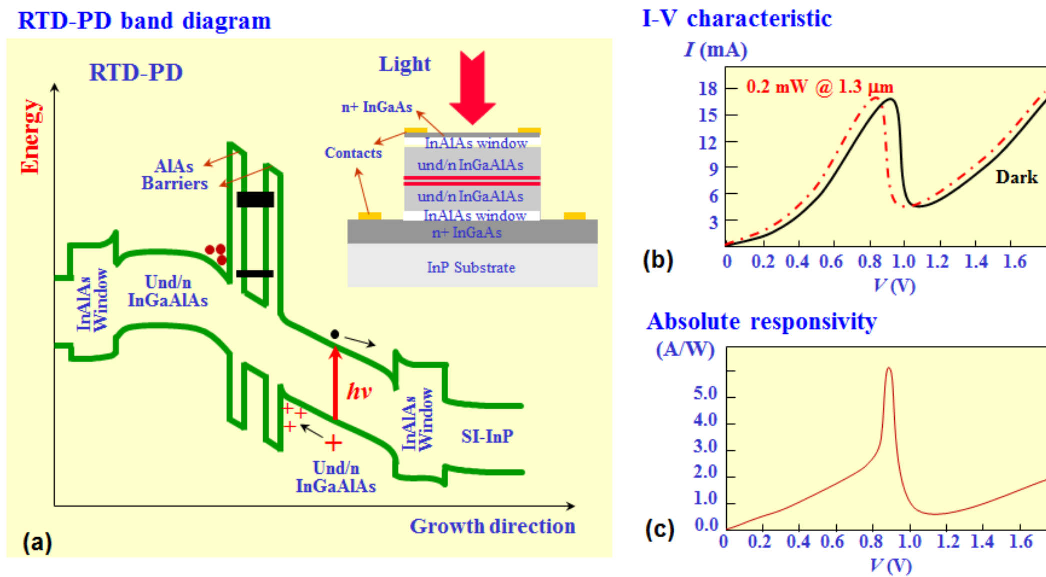

Figure 6: (a) Schematic of the band energy diagram of a surface illuminated InGaAlAs/AlAs RTD-PD. Inset is shown a representation of the RTD-PD mesa cross-section. (b) Typical dark and illuminated I-V characteristics for moderate illumination. (c) Absolute responsivity as function of the applied bias.

The light-generated holes in the collector region of the device leads to an enhancement of electric field across the DBQW and the adjacent collector region, which leads to a global shift of the I-V to lower voltage with an additional current increase, which is dependent on the optical power levels being absorbed. Moreover, due to the internal electrical field dependence the device responsivity (the ratio between the photocurrent and the optical power absorbed) becomes a function of the bias voltage and the power level. Figure 7 shows the typical optical response of RTD-PDs for different optical power levels at the wavelength 1310 nm.

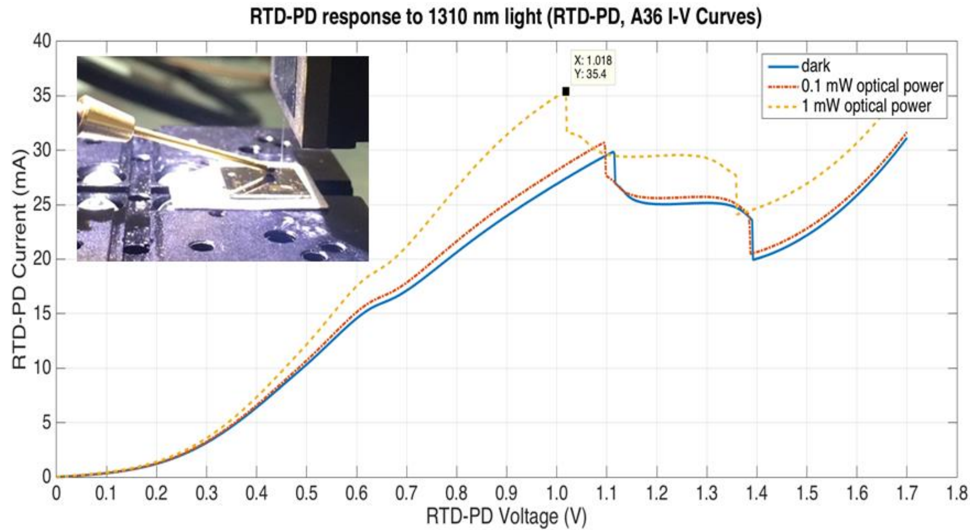

Figure 7: Typical response of RTD-PDs for different optical power levels at the wavelength 1310 nm. The steady state responsivity in the first positive differential conductance region can reach tens of A/W.

RTD-PDs can be operated either in the steady state mode (when polarized in one of the positive differential conductance (PDC) regions of the I-V curve), or in the oscillatory mode (when polarized in the NDC region). These modes of operation and the RTD-PDs functionalities make them potential candidates for implementation of low cost highly efficient optical-to-wireless interfaces capable of transferring electrical signals embedded in the optical carriers used in fibre optic communications to mm-wave/THz carriers. Moreover, when directly illuminated by low power intensity modulated optical signals the RTD-PD oscillators can lock to the optical signals subcarriers, with the RTD-PD electrical output power being merely determined by the NDC region characteristics. Indeed, microwave optoelectronic RTD-PD oscillators with record RF output powers over 10 mW around the X-band have recently been demonstrated on iBROW and are being characterized for these functionalities, details of which will be reported elsewhere.

Besides, then polarized in the PDCs but close to the NDC, the RTD circuits can behave as excitable systems: when undisturbed RTDs remain in the quiescent (equilibrium) states, producing a small response to a “small” perturbation (stimulus) but fire a large transient response when the small perturbation (stimulus) exceeds a certain threshold then settling back to the quiescent point in what is called the refractory period, after which the RTDs can be excited again. Moreover, for small perturbations away from the equilibrium, the return is monotonic; however, for perturbations beyond a threshold value, the return is not monotonic, but undergoes a large excursion before settling down. The excitability properties make intensity modulated optical signals capable to induce RTD-PD transition from the peak to the valley, producing electrical signals that mimic the optical signals subcarriers.

Optimized RTD-PDs for operation at 1550 nm are currently under development. With such structures we expect to achieve: i) the reduction of the optical power levels required to ensuring that the system can be driven by an optical subcarrier RF signal (obtained larger light signal detection dynamic range); ii) the maximization of the optical-electrical power gain; iii) significant improvement of linearity and spectral response; v) an enhancement of differential responsivity (sensitivity) and responsivity-gain product.

6. CONCLUSION

An RTD oscillator design methodology to provide high power and high oscillation frequency was described in this paper. All the circuit components including the RTD devices are large and can be easliy fabricated using photolithography. The approach was demonstrated up to ~0.3 THz with practically relevant output powers of up to 0.5 mW. Theorical estimation shows that ~1.4 THz could be achieved with using the same approach through lower resistance Ohmic contacts, while optimised epitaxial designs and oscillator designs/layouts are expected to yield at least 1 mW output power at 0.3 THz. Indeed, 1 mW RTD sources in the J-band has already been demonstrated by the group using a synchronisation power combinining circuit[34] and results will be published elsewhere soon. Optoelectronic

properties of RTDs have also been described. Future work will aim at improved designs and at integrating the oscillators with suitable antennas, and in employing them in prototype application scenarios.

REFERENCES

[1] Tonouchi, M., "Cutting-edge terahertz technology," Nature Photonics1, 97–105 (2007).

[2] Hosako, I., *et al.*, "At the dawn of a new era in terahertz technology," Proc. IEEE, 95(8), 1611-1623 (2007).

[3] Siles, J. V. and Grajal, J., "Physics-based design and optimization of Schottky diode frequency multipliers for terahertz applications," IEEE Trans. on Microwave Theory and Techn., 58(7), 1933-1942 (2010).

[4] Malko, A., Bryllert, T., Vukusic, J. and Stake J., "A 474 GHz HBV frequency quintupler integrated on a 20 m thick silicon substrate," IEEE Trans. THz Sci. Technol., 5(1), pp. 85–91 (2015).

[5] Li L., Chen, L., Zhu, J., Freeman, J., Dean, P., Valavanis, A., Davies, A. G. and Linfield, E. H., "Terahertz quantum cascade lasers with >1 W output powers," Electronics Letters, 50(4), 309–311 (2014).

[6] Melo, A. M., *et al.*, "Imaging at 0.2 and 2.5 terahertz," Proc. SPIE, Terahertz, RF, Millimeter, and Submillimeter-Wave Technology and Applications VI, 8624, 86240E-1-6 (2013).

[7] Razeghi, M., "Quantum cascade lasers for IR and THz spectroscopy," SPIE Newsroom, 005239 (2013).

[8] Sollner, T., Goodhue, W. D., Tannenwald, P. E., Parker, C. D. and Peck, D. D., "Resonant tunneling through quantum wells at frequencies up to 2.5 THz," Appl. Phys. Lett., 43, 588–590 (1983).

[9] Maekawa, T., Kanaya, H., Suzuki, S. and Asada, M., "Oscillation up to 1.92 THz in resonant tunneling diode by reduced conduction loss," Applied Physics Express, 9(2), 024101, (2016).

[10] Feiginov, M., Kanaya, H., Suzuki, S. and Asada, M., "1.46 THz RTD oscillators with strong back injection from collector," in International Conference on Infrared, Millimeter and Terahertz Waves (2014).

[11] Okada, K., Kasagi, K., Oshima, N., Suzuki, S. and Asada, M., "Resonant-tunneling-diode terahertz oscillator using patch antenna integrated on slot resonator for power radiation," IEEE Transactions on Terahertz Science and Technology, 5(4), 613-618 (2015).

[12] Lee, J., Kim, M. and Yang, K., "A 1.52 THz RTD triple-push oscillator with μW-level output power," in IEEE Transactions on Terahertz Science and Technology, 6(2), 336-340 (2016).

[13] Feiginov, M., Sydlo, C., Cojocari, O. and Meissner, P., "Resonant-tunnelling-diode oscillators operating at frequencies above 1.1 THz," Appl. Phys. Lett. 99, 233506-1-3 (2011).

[14] Kanaya, H., Shibayama, H., Sogabe, R., Suzuki, S. and Asada, M., "Fundamental oscillation up to 1.31 THz in resonant tunneling diodes with thin well and barriers", Appl. Phy. Express,5, 124101 (2012).

[15] Shiode, T., Mukai, T., Kawamura, M. and Nagatsuma, T., "Giga-bit wireless communication at 300 GHz using resonant tunneling diode detector," Asia–Pacific Microw. Conf., 1122–1125 (2011).

[16] Ishigaki, K., *et al.*, "Direct intensity modulation and wireless data transmission characteristics of terahertz-oscillating resonant tunnelling diodes," Electron. Lett., 48(10), 582–583 (2012).

[17] Ikeda, Y., Kitagawa, S., Okada, K., Suzuki, S. and Asada, M., "Direct intensity modulation of resonant-tunneling-diode terahertz oscillator up to ∼ 30 GHz." IEICE Electronics Express, 12(3), 20141161 (2015).

[18] Jacobs, K. J. P., Stevens, B. J., Wada, O., Mukai, T., Ohnishi, D. and Hogg, R. A., "A Dual-pass high current density resonant tunneling diode for terahertz wave applications," IEEE Electron Device Letters, 36(12), 1295 - 1298 (2015).

[19] Hinata, K., Shiraishi, M., Suzuki, S. and Asada, M., "High power THz oscillators with offset-fed slot antenna and high current density resonant tunneling diodes," in International Conference on Infrared, Millimeter, and Terahertz Waves, 1-2 (2009).

[20] Suzuki, S., Shiraishi, M., Shibayama, H. and Asada, M., "High-power operation of terahertz oscillators with resonant tunneling diodes using impedance-matched antennas and array configuration", IEEE J. Selected Topics Quantum Electronics, 19(1), 8500108 (2013).

[21] Templ, W., and Pascht, A., "Perspectives for commercialisation of RTDs in high performance mmWave transceivers," Workshop on Compact and High-Performance Millimetre-wave and Terahertz Sources/Systems, European Microwave Week (2016).

[22] Hoppe, R., Rose, D. M., Wahl, R., Wölfle, G. and Kürner, T., "Simulator for the analysis of the mutual impact between indoor femtocells and urban macrocells," 6th European Conference on Antennas and Propagation (EuCAP 2012), Prague, Czech Republic (2012).

[23] Wang, J., Wang, L., Li, C., Romeira, B., and Wasige, E., "28 GHz MMIC Resonant tunneling diode oscillator of around 1mW output power," Electronics letters, 49(13), 816-818 (2013).
[24] Wang, J., Wang, L., Li, C., Alharbi, K., Khalid, Ata., and Wasige, E., "W-band InP-based resonant tunnelling diode oscillator with milliwatt output power," 26th International Conference on Indium Phosphide and Related Materials, Montpellier, France, May (2014).
[25] Wang, J., Alharbi, K., Ofiare, A., Zhou, H., Khalid, Ata., Cumming, D. and Wasige, E., "High performance resonant tunneling diode oscillators for THz applications." IEEE Compound Semiconductor Integrated Circuit Symposium (CSICS), 1-4, (2015).
[26] Reddy, M., "Schottky-collector resonant tunnel diodes for sub-millimeter-wave applications," PhD Thesis, University of California Santa Barbara (1997).
[27] Wang, L., ''Reliable design of tunnel diode and resonant tunnelling diode based microwave and millimeterwave sources," Ph.D. Thesis, University of Glasgow (2010).
[28] Schulman, J. N., De Los Santos, H. J. and Chow, D. H., "Physics-based RTD current-voltage equation," IEEE Electron Device Lett., 17(5), 220–222 (1996).
[29] Liu, Q., Seabaugh, A., Chahal, P. and Morris, F. J., "Unified AC model for the resonant tunneling diode," IEEE Trans. Electron Devices, 51(5), 653–657 (2004).
[30] Chow, D. H., Schulman, J. N., Özbay, E. and Bloom, D. M., "Investigation of In0.53Ga0.47As/AlAs resonant tunneling diodes for high speed switching, " Appl. Phy. Lett., 61(14), 1685-1687 (1992).
[31] Shao, C., Dasmahapatra, P., Sexton, J., Missous, M. and Kelly, M. J., "Highly reproducible tunnel currents in MBE-grown semiconductor multilayers," Electronics Letters, 48(13), 792-794 (2012).
[32] Dasmahapatra, P., Sexton, J., Missous, M., Shao, C. and Kelly, M. J., "Thickness control of molecular beam epitaxy grown layers at the 0.01–0.1 monolayer level," Semicond. Science and Technol., 27(8), 085007 (2012).
[33] Singisetti, U., Crook, A. M., Lind, E., Zimmerman, J. D., Wistey, M. A., Gossard, A. C. and Rodwell, M. J. W., "Ultra-Low Resistance Ohmic Contacts to InGaAs/InP," 65th Annual Device Research Conference (2007).
[34] Alharbi, K. H., "High performance terahertz resonant tunnelling diode sources and broadband antenna for air-side radiation," PhD Thesis, University of Glasgow (2016).
[35] Khalid, A., Li, C., Lok, L. B. and Cumming, D. R. S., "Oscillation detection technique by using vector network analyzer," Journal of Terahertz Science and Electronic Information Technology, 13(3), 382-388 (2015).
[36] Wang, L., Figueiredo, J. M. L., Ironside C. N. and Wasige, E., "DC characterization of tunnel diodes under stable non-oscillatory circuit conditions," IEEE Transactions on Electron Devices, 58(2), 343-347 (2011).
[37] Zeinolabedinzadeh, S., Song, P., Kaynak, M., Kamarei, M., Tillack, B. and Cressler, J. D., "Low phase noise and high output power 367 GHz and 154 GHz signal sources in 130 nm SiGe HBT technology," IEEE MTT-S International Microwave Symposium, 1-4 (2014).
[38] Khalid, A., *et al.*, and Cumming, D. R. S., "Terahertz oscillations in an $In_{0.53}Ga_{0.47}As$ submicron planar Gunn diode," Journal of. Applied Physics., 115, 114502 (2014).
[39] Seo, M., Urteaga, M., Young, A., Jain, V., Griffith, Z., Hacker, J., Rowell, P., Pierson, R. and Rodwell, M., ">300 GHz Fixed frequency and voltage-controlled fundamental oscillators in an InP DHBT process," Proc. Int. Micro. Symp., 272-275 (2010).
[40] Tousi, Y., "A Novel CMOS high-power terahertz VCO based on coupled oscillators: theory and implementation," IEEE Journal of Solid-State Circuits, 47(12), 3032-3042 (2012).
[41] Asada, M., and Suzuki, S., "Compact THz oscillators with resonant tunneling diodes and application to high-capacity wireless communications," Int. Conf. on Applied Electromagnetics and Communications (ICECom), 1-5 (2013).
[42] Crook, A. M., Lind, E., Griffith, Z., Rodwell, M. J. W., Zimmerman, J. D., Gossard, A. C. and Bank, S. R., "Low resistance, nonalloyed Ohmic contacts to InGaAs," Applied Physics Letters, 91(19), 192114 (2007).
[43] Romeira, B., Pessoa, L., *et al.*, and Figueiredo, J. M. L., "Photo-detectors integrated with resonant tunneling diodes," Sensors, 13(7), 9464-9482 (2013).
[44] Pfenning, A., Hartmann, F., Langer, F., Kamp, M., Höfling, S. and Worschech, L., "Sensitivity of resonant tunneling diode Photodetectors," Nanotechnology 27, 355202 (9pp) (2016).
[45] Dong, Y., Xu, J., Wang, G., Ni, H., Pei, K., Chen, J., Gao, F., Li, B. and Niu, Z., "Resonant tunnelling diode photodetector operating at near-infrared wavelengths with high responsivity," Electronics Letters, 51(17), 1355–1357 (2015).